ECS Journal of Solid State Science and Technology, **3** (10) R173-R184 (2014)
2162-8769/2014/3(10)/R173/12/$31.00 © The Electrochemical Society

Vacuum Referred Binding Energy of the Single 3d, 4d, or 5d Electron in Transition Metal and Lanthanide Impurities in Compounds

E. G. Rogers and P. Dorenbos[z]

Delft University of Technology, Faculty of Applied Sciences, Department Radiation Science and Technology (FAME-LMR), 2629 JB Delft, Netherlands

The vacuum referred binding energy (VRBE) of the single electron in the lowest energy 3d level of Sc^{2+}, V^{4+}, Cr^{5+}, the lowest 4d level of Y^{2+}, Zr^{3+}, Nb^{4+}, Mo^{5+} and the lowest 5d level of Ta^{4+}, and W^{5+} in various compounds are determined by means of the chemical shift model. They will be compared with the VRBE in the already established lowest 3d level of Ti^{3+} and the lowest 5d level of Eu^{2+} and Ce^{3+}. Clear trends with changing charge of the transition metal (TM) cation and with changing principle quantum number $n = 3$, 4, or 5 of the *nd* level will be identified. This work will demonstrate that the trends correlate with the VRBE in the free ion *nd* TM cation level. The acquired knowledge on the VRBE of the electron in the *nd* TM impurity levels but also on TM based compounds with *nd* type of conduction band bottom provides new insight in the luminescence properties of TM activated compounds.

Manuscript submitted May 23, 2014; revised manuscript received July 22, 2014. Published August 7, 2014.

We live in a world where energy and resource efficiencies are becoming more and more important. Optimized luminescent materials are required for light emitting diodes of the correct hue,[1–4] to improve the efficiency of solar cells,[5–7] to make longer lasting and brighter "glow in the dark" phosphors,[8–10] and for faster, brighter, more proportional scintillators for particle and astro- physics, medical imaging and homeland security,[11–14] and this is all needed with resources that may be limited by physical availability or global politics.[15–18] It is neccessary therefore to find improved and/or alternative luminescent materials. The use of ab initio or semi-empirical models to predict the optical properties and electronic structures of luminescent materials are important in aiding this work, see e.g. Refs. 19–22. Such models may be used to identify areas of interest, for instance identifying a promising new combination of host compound and dopant ion. They may also be used in a systematic study of whole families of compounds in order to gain new understanding of the underlying physics,[21,23] or to better understand the performance of an existing luminescent material.

The location of lanthanide impurity levels in inorganic compounds has been a subject of interest for many years. In 2003 Dorenbos introduced a semi-empirical model to determine the electron binding energies in the 4f and 5d levels of lanthanides relative to the energy at the top of the host valence band in inorganic compounds.[25] More recently a chemical shift model was introduced that models the electron binding energy in lanthanide doped compounds relative to the vacuum level.[20] In a recent paper we showed that the same model can be applied to Ti^{4+} doped compounds by using the energy of the O^{2-} to Ti^{4+} charge transfer transition.[26] This allowed us to directly compare the vacuum referred binding energy (VRBE) of an electron in the lowest energy $3d_1$ level of Ti^{3+} in a compound with the VRBE of a lanthanide level in the same compound.

In this work we collected data on the $3d^0$ transition metals (TM), Sc^{3+}, V^{5+}, Cr^{6+}, the $4d^0$ TM Zr^{4+}, Nb^{5+}, Mo^{6+} and the $5d^0$ TM Ta^{5+}. These TM cations can be utilized as activators in luminescent materials but also as constituents of host compounds activated with lanthanides or other TMs. Excitation of an electron from the valence band into the empty nd^0 orbital results in a nd^1 one-electron state. Such a situation is similar to when a 4f electron is excited to the 5d level of lanthanide ions such as Ce^{3+}, Tb^{3+} and Eu^{2+}. One may then compare the VRBE of an electron in the lowest energy $3d_1$ level, the lowest energy $4d_1$ level and the lowest energy $5d_1$ level of transition metal and lanthanide ions. The periodic table-like illustration of Fig. 1 already reflects the main results of this work. The number in the right hand corner for each element in the table represents the VRBE of an electron in the lowest energy nd_1 level as averaged over different compounds. One may notice clear trends with changing charge Q = 2+, 3+, 4+, or 5+ of the TM or lanthanide, and with changing principle quantum number n=3, 4, or 5.

Methodology

Figure 2 summarizes the notation used to describe the optical transitions of relevance in this article. Ti^{4+} is used in Fig. 2 to represent the transition metals while Ce^{3+}, Eu^{3+} and Pr^{3+} are used to represent the lanthanides. Energies are expressed relative to the vacuum level (E_{vac}) which is the energy of an electron at rest in the vacuum. Lanthanide spectroscopy, combined with the chemical shift model, is used to place the energy of the top of the valence band relative to the vacuum. In order to attain a clear and consistent labeling system for the many different transitions and energies, the following notation is used: $E_{sub}^{sup}(n, Q)$, where n is the number of electrons in the 4f, 3d, 4d or 5d shell and Q represents the valency of the lanthanide or transition metal. A superscript denotes the type of transition involved while a subscript displays the type of levels involved. In order to create a VRBE scheme we need two things, a reference point, that is a known

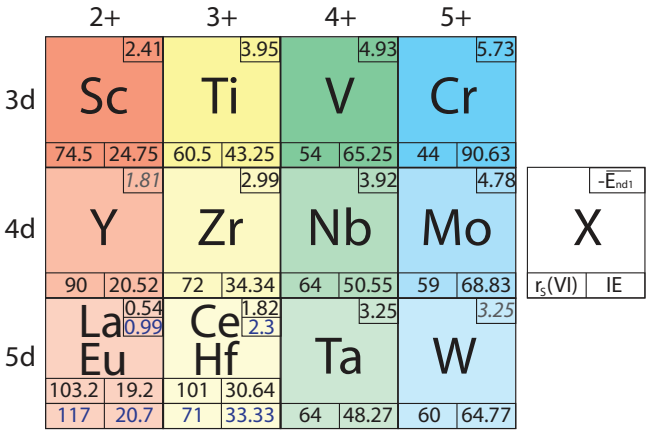

Figure 1. Schematic of the properties of the transition metal (TM) and lanthanide impurities studied in this work. $\overline{E_{nd1}}$ in each right top corner is the vacuum referred binding energy of the electron in the lowest nd_1 level for a TM or lanthanide impurity as averaged over various compounds in eV, r_S in the left bottom corner is the Shannon ionic radius for VI coordinated ions[24] in pm, and IE in the right bottom corner is the 3rd, 4th, 5th or 6th ionization energy of the free TM in eV. The 2nd and 3rd ionization energies for the three lanthanides were corrected for the $4f_{gs}$-$5d_1$ energy difference to obtain the binding energy of the excited 5d electron. Italic numbers are estimates.

[z]E-mail: p.dorenbos@tudelft.nl

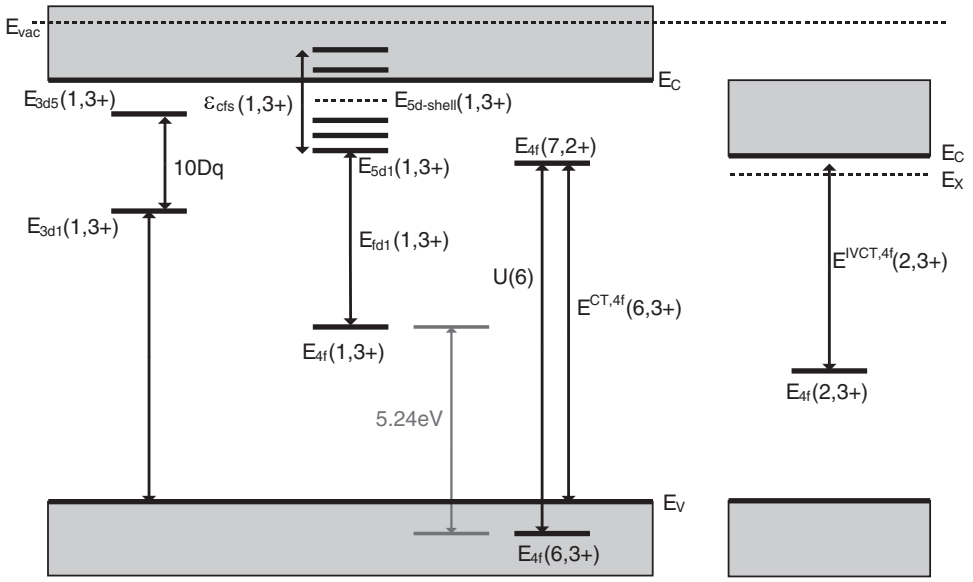

Figure 2. Examples of the different optical transitions employed to construct the energy level schemes and the notation used to indicate binding energies and transitions in this work.

energy relative to the vacuum, and a way of placing the other levels relative to this reference. When using the chemical shift model to place the VRBE, $E_{4f}(7, 2+)$, the energy of the Eu^{2+} 4f ground state, will be used as the reference. In principle one might equally well use the 4f ground state of any of the other lanthanides, thanks to the well known and well defined binding energy relationship between them.

In order to determine the VRBE $E_{4f}(7, 2+)$, the coulomb repulsion energy $U(6)$ is needed which is defined as

$$U(6) \equiv E_{4f}(7, 2+) - E_{4f}(6, 3+) \quad [1]$$

that is, the difference between the binding energy of an electron in the Eu^{2+} and Eu^{3+} ground state as shown in Fig. 2. $U(6)$ can be estimated to an accuracy of about ±0.1 eV from the centroid shift $\epsilon_c(1, 3+)$ of the Ce^{3+} 5d levels using the empirical relationship[27]

$$U(6) = 5.44 + 2.834e^{-\epsilon_c(1,3+)/2.2}. \quad [2]$$

The Chemical shift model provides the relationship between $U(6)$ and $E_{4f}(7, 2+)$

$$E_{4f}(7, 2+) = -24.92 + \frac{18.05 - U(6)}{0.777 - 0.0353U(6)}. \quad [3]$$

The charge transfer energy $E^{CT,4f}(6, 3+)$ can then be used to place the valence band relative to $E_{4f}(7, 2+)$. When this information is unavailable, one may use the Pr^{3+} ($E^{IVCT,4f}(2, 3+)$) or Tb^{3+} ($E^{IVCT,4f}(8, 3+)$) intervalence charge transfer (IVCT) energy. An electron is then transferred from the Ln^{3+} ground state to conduction band related states. The transition is illustrated in the right side panel of Fig. 2, and we will assume that the transition ends at an energy in between E_X and E_C as in Ref. 28.

VRBE in the $3d_1$ level of Sc^{2+}, Ti^{3+}, V^{4+} and Cr^{5+}

In Ref. 26 the Ti^{3+} VRBE $E_{3d1}(1, 3+)$ was determined in about forty different host compounds. The average $\overline{E_{3d1}(1, 3+)} = -3.95 \pm 0.07$ eV, and individual data points scatter about 1 eV around this average, attributed mainly to the host dependent crystal field splitting of the 3d levels. A similar amount of scatter is observed for the VRBE of the electron in the Ce^{3+} $5d_1$ level, see Ref. 26 and Fig. 10 further on in this article. In this section the $3d^0$ TMs Sc^{3+}, V^{5+} and Cr^{6+} as dopants in compounds are studied in order to determine the VRBE of the electron in the $3d_1$ level of Sc^{2+}, V^{4+}, and Cr^{5+}. Sc^{3+} can be found as a constituent of the host crystal but also as a dopant in compounds. Table I contains the data, together with the references, used to create the stacked band scheme of Fig. 3. E^{ex} is the energy needed to create the host exciton at low temperature (≈10 K). $E^{CT,4f}$ is the Eu^{3+} $E^{CT,4f}(6,3+)$ charge transfer energy. This in

Table I. Experimental, and within brackets estimated or derived, data required for construction of VRBE schemes with the Sc^{2+} $3d^1$ level. All energies are in eV.

Host	E^{ex}	$E^{CT,4f}$	$E^{CT,3d}$	U	E_V	E_C	E_{3d_1}
$GdAl_3(BO_3)_4$	7.55[29–31]	4.9[30–34]	6.09[35]	7.02	− 8.98	− 0.83	− 2.89
$YAl_3(BO_3)_4$	7.65[29,30,36,37]	5.15[36,38,39]	7[40]	7.03	− 9.24	− 0.97	− 2.24
YBO_3	7.55[41]	5.59[41]	7.32[42]	6.85	− 9.58[41]	− 1.43	− 2.26
c-$LuBO_3$	8.15[41]	5.08[41]	6.89[43]	6.94	− 9.12[41]	− 0.32	− 2.23
Al_2O_3	9[44]	(5.7)[44]	8[45]	(7.06)	− 9.8[44]	− 0.08	− 1.8
$Y_3Al_5O_{12}$	7.1[46]	5.42[46]	6.67[47]	6.77	− 9.38[46]	− 1.71	− 2.71
$YAlO_3$	7.96[41]	5.06[41]	7.41[48]	6.81	− 9.04[41]	− 0.44	− 1.63
$Lu_3Al_5O_{12}$ (Lu site)	7.35[46]	5.65[46]	6.89[49,50]	6.66	− 9.6[46]	− 1.66	− 2.71
$Lu_3Al_5O_{12}$ (Al site)	7.35[46]	5.65[46]	7.34[49]	6.66	− 9.6[46]	− 1.66	− 2.26
Y_2O_3	6.1[41]	5.1[41]	5.84[51]	6.47	− 8.91[41]	− 2.32	− 3.07
$ScPO_4$	7.45[41]	6[41]	7.45[41]	(7.06)	− 10.1[41]	− 2.05	− 2.65
$ScBO_3$	7.2[41]	5.5[41]	7.2[41]	6.86	− 9.5[41]	− 1.72	− 2.3
Sc_2O_3	6.3[41]	(5.2)[41]	6.3[41]	6.51	− 8.93[41]	− 2.13	− 2.63

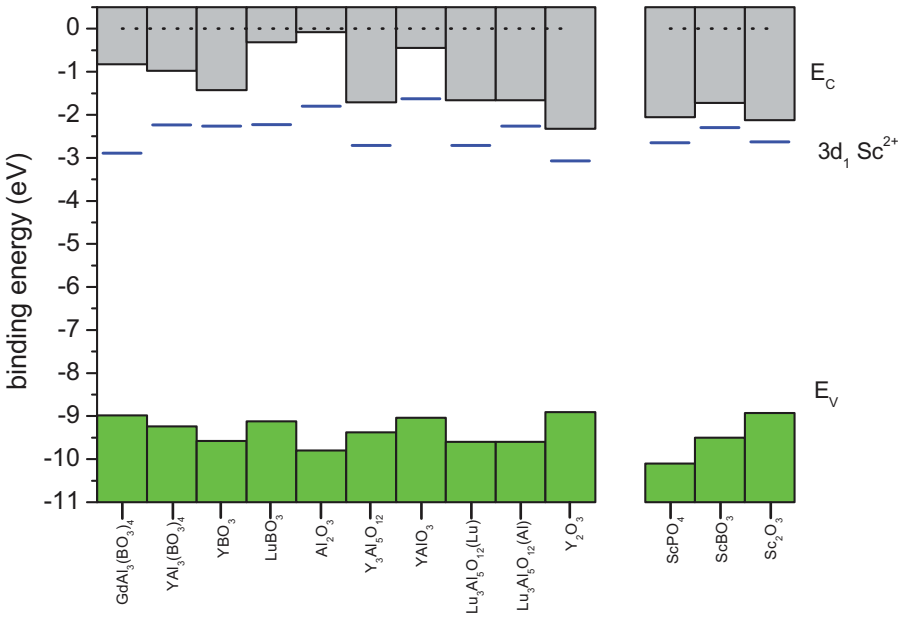

Figure 3. Stacked VRBE schemes for Sc^{3+} doped compounds. The top of the green bars indicate the VRBE E_V at the top of the valence band while the bottom of the gray bars indicate the VRBE E_C at the bottom of the conduction band. Blue horizontal lines denote the VRBE in the Sc^{2+} $E_{3d1}(1, 2+)$ level.

combination with $E_{4f}(7, 2+)$, derived from the $U(6)$ values in column 5, is used to determine the VRBE at the top of the valence band E_V (column 6). By adding the electron-hole binding energy E^{ex}_{e-h} of the exciton to $E_X \equiv E_V + E^{ex}$, the VRBE E_C at the bottom of the conduction band is reached (column 7). For wide bandgap compounds the estimated value $E^{ex}_{e-h} = 0.08 \times E^{ex}$ was used. For small bandgap compounds or compounds with high dielectric constants the binding energy will be a smaller fraction of E^{ex}. For most of the compounds above data were already presented in previous work. For other compounds an account on how data was obtained is provided in Appendix A. New in this work is the compilation of the valence band to Sc^{3+} charge transfer energy $E^{CT,3d}$ (column 4). Together with E_V it provides the VRBE $E_{3d1}(1, 2+) = E_V + E^{CT,3d}(1, 3+)$ of the electron in the lowest $3d_1$ level of Sc^{2+} (column 8). It is assumed that, like for Eu^{2+}, the energy of CT provides a good measure for the location of the Sc^{2+} level above E_V. Table I also contains information on three Sc^{3+}-based compounds. For these compounds, the VRBE E_X is considered to be equivalent to the VRBE $E_{3d1}(1, 2+)$.

Figure 3 shows a stacked VRBE diagram of the different compounds of Table I together with the VRBE of the electron in the lowest energy Sc^{2+} $3d_1$ level. The top of the valence band in the oxide compounds is always near -9 to -10 eV. The average $\overline{E_{3d1}(1, 2+)} = -2.41 \pm 0.11$ eV, and the Sc^{2+} level energy spreads about $\pm$ 0.8 eV around this average which is mostly attributed to compound to compound variations in the crystal field splitting of the 3d-levels. The bottom of the conduction band is found between 0 and -2 eV. The relatively small binding energy in the Sc^{2+} $3d_1$ level means that it is very difficult to stabilize the Sc^{2+} valence in compounds and very few reports can be found on Sc^{2+}. Nevertheless, knowledge on $E_{3d_1}(1, 2+)$ is still important since Sc^{3+} may act as an electron trap as long as $E_{3d_1}(1, 2+) < E_C$.

Table II. Experimental, and within brackets estimated or derived, data required for construction of VRBE schemes with the V^{4+} $3d^1$ level. All energies are in eV.

Host	E^{ex}	$E^{CT,4f}$	$E^{CT,3d}$	U	E_V	E_C	E_{3d_1}
$CaSO_4$	8.45[52,53]	4.77[54,55]	4.43[56]	7.19	− 8.94	0.19	− 4.51
$GdPO_4$	8.05[41]	5.14[41]	4.03[57]	(7.15)	− 9.28[41]	− 0.59	− 5.25
YPO_4	8.55[41]	5.65[41]	4.4[58]	7.09	− 9.77[41]	− 0.54	− 5.37
$LuPO_4$	8.6[41]	5.74[41]	4.19[59]	7.08	− 9.85[41]	− 0.56	− 5.66
SiO_2	8.7[26]	(5.53)[26]	4.2[60]	(7.0)	− 9.6[26]	− 0.2	− 5.4
GeO_2	5.9[61]		3.8[62]	N/A	− 8.8±0.2	− 2.4	− 5
SnO_2	3.59[63]	3.79[63]	2.78[64]	6.8	− 7.76[63]	− 3.88	− 4.98
Mg_2SiO_4	7.8[65,66]	4.86[67,68]	4.65[69]	(6.8)	− 8.78	− 0.36	− 4.13
$ZrSiO_4$	7.1[70]	4.63[71]	3.97[72]	(6.9)	− 8.6	− 1.25	− 4.63
Al_2O_3	9[44]	(5.7)[44]	4.04[60]	(7.06)	− 9.8[44]	− 0.08	− 5.76
$Gd_3Al_5O_{12}$	6[46]	5[46]	4.13[73]	6.77	− 8.96[46]	− 2.48	− 4.83
$Y_3Al_5O_{12}$	7.1[46]	5.42[46]	4.34[74]	6.77	− 9.38[46]	− 1.71	− 5.04
$CaYAlO_4$	6[75]	4.56[26]	3.76[76]	(6.7)	− 8.8±0.3	− 2.32	− 5.04
$MgAl_2O_4$	6.9[26]	4.4[26]	3.98[77]	(6.80)	− 8.37[26]	− 0.92	− 4.39
$LiNbO_3$	4.7[26]	(4.7)[26]	3.81[78]	(6.8)	− 8.67[26]	− 3.59	− 4.86
$LaNbO_4$	4.84[79]	(4.49)[80]	4.02[81]	(6.8)	− 8.76	− 3.47	− 4.74
TiO_2	3.45[63]	3.8[63]	2.89[82]	(6.7)	− 7.72[63]	− 3.99	− 4.83
$SrTiO_3$	3.46[63]	3.42[63]	2.52[83]	(6.7)	− 7.34[63]	− 3.6	− 4.82
$CaTiO_3$	3.85[63]	4.1[63]	2.95[84]	6.7	− 8.02[63]	− 3.86	− 5.07
ZrO_2	5.35[85]	4.43[85]	3.35[86]	(6.6)	− 8.3[85]	− 2.52	− 4.95
HfO_2	5.85[85]	4.43[85]	4.07[87]	(6.6)	− 8.3[85]	− 2.01	− 4.23

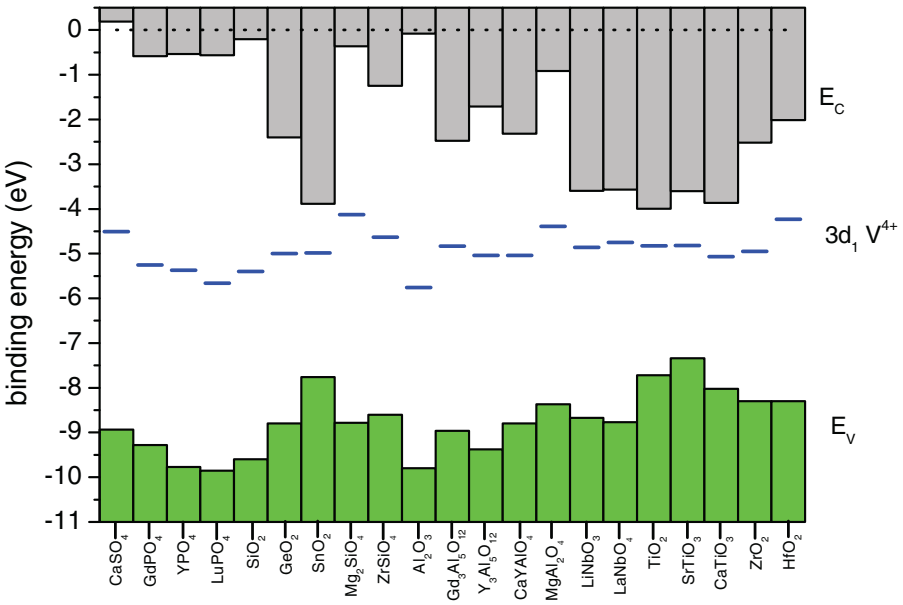

Figure 4. Stacked VRBE schemes for V^{5+} doped compounds. The top of the green bars indicate the VRBE E_V at the top of the valence band while the bottom of the gray bars indicate the VRBE E_C at the bottom of the conduction band. Blue horizontal lines denote the VRBE in the V^{4+} $E_{3d1}(1, 4+)$ level.

The VRBE of an electron in the Ti^{3+} $3d_1$ level is about 1.5 eV more negative than that in Sc^{2+}. As a result Ti^{3+} is more stable in compounds than Sc^{2+}. Stability is increased even further for V^{4+}. Table II and Fig. 4 contain and display data on the VRBE $E_{3d1}(1, 4+)$ of an electron in the lowest V^{4+} $3d_1$ level. It is on average -4.93 ± 0.09 eV with a data spread of $\pm$ 0.8 eV. Due to the much lower VRBE than that for Sc^{2+} information can be obtained on compounds with much lower E_C like TiO_2, SnO_2 and $CaTiO_3$.

Finally in Table III data on the highly charged Cr^{6+} ion are collected, which are required to construct Fig. 5. The largest energy for the charge transfer to Cr^{6+} is observed for the fluoride $LiSrAlF_6$. Figure 5 shows that the large value is entirely caused by the low lying E_V due to the strong binding of an electron in the fluorine ligand. The VRBE of the electron in the $3d_1$ level of Cr^{5+} in $LiSrAlF_6$ at -5.98 eV ends up close to the average VRBE $\overline{E_{3d1}(1, 5+)} = -5.73 \pm 0.14$eV. Like for the other $3d_1$ levels the individual data spread $\pm$ 0.7 eV around the average. Comparing the results for Sc^{2+}, Ti^{3+}, V^{4+}, and Cr^{5+}, we find that the VRBE of an electron in the $3d_1$ impurity state decreases continuously from -2.41 eV, -3.95 eV, -4.93 eV, and -5.73 eV with higher charge of the TM.

VRBE in the $4d_1$ level of Y^{2+}, Zr^{3+}, Nb^{4+} and Mo^{5+}

In this section we will determine or estimate the VRBE of an electron in the lowest $4d_1$ levels of Y^{2+}, Zr^{3+}, Nb^{4+}, and Mo^{5+}. It will turn out that on average the binding energies in the $4d_1$ levels are less than in the $3d_1$ levels when comparing the 3d and 4d TMs of the same valence. The binding energy in the Y^{2+} $4d_1$ level is therefore less than in the Sc^{2+} level which brings the Y^{2+} ground state, in a vast majority of compounds, inside the conduction band. This immediately explains why Y^{3+}, the $4d^0$ analog of Sc^{3+}, is rarely seen as a dopant in compounds. It will be optically inactive, a CT band will not be observed and it is also not capable of trapping an electron. Yet, to make an estimate on $E_{4d1}(1, 2+)$ we will utilize data on yttrium based compounds where the bottom of the conduction band contains a large contribution from Y^{2+} 4d orbitals. Figure 6 shows a stacked band diagram from published VRBE data on Y^{3+}-based host lattices in Refs. 26, 41, 46, and 114. Like for Sc^{3+}-based compounds the value for E_X is used as estimate for the Y^{2+} $E_{4d1}(1, 2+)$ VRBE. These data show $\pm$ 1 eV spread around the average $\overline{E_{4d1}(1, 2+)} = -1.81 \pm 0.15$ eV which is indeed above the binding energy for the $3d_1$ level in Sc^{2+}. The $\overline{E_{4d1}(1, 2+)}$ for Y^{2+} in $Y_3Al_5O_{12}$ and $Y_3Ga_5O_{12}$ lies well below $\overline{E_{4d1}(1, 2+)}$ and that for $YAlO_3$ lies well above. These deviations are clearly related to the well known exceptionally large crystal field splitting in garnet compounds and the relatively small splitting in the yttrium perovskite.

The electron in the Zr^{3+} $4d_1$ level will be stronger bonded than that in the Y^{2+} $4d_1$ level and now one may find information on the energy of charge transfer to Zr^{4+} dopants in compounds. Table IV contains such data from 5 different compounds. In addition data are compiled on Zr-based compounds where the conduction band bottom is composed mainly from Zr 4d orbitals. The data are displayed as a stacked band scheme in Fig. 7. The average $\overline{E_{4d1}(1, 3+)} = -2.99 \pm 0.12$ eV with a spread of about 0.7 eV. The average value is smaller than for Y^{2+} but

Table III. Experimental, and within brackets estimated or derived, data required for construction of VRBE schemes with the Cr^{5+} $3d^1$ level. All energies are in eV.

Host	E^{ex}	$E^{CT,4f}$	$E^{CT,3d}$	$U(6)$	E_V	E_C	E_{3d_1}
$LiSrAlF_6$	11.2[88,89,90]	7.9[91]	6.35[92]	7.69	− 12.33	− 0.23	− 5.98
$Li_2B_4O_7$	8.2[93]	5.04[94]	3.46[95]	7.2	− 9.19	− 0.33	− 5.73
SiO_2	8.7[26]	(5.53)[26]	3.44[96]	(7.0)	− 9.6[26]	− 0.2	− 6.16
Li_2CaSiO_4	7.55[97]	4.77[98,99]	3.26[100]	6.92	− 8.80	− 0.64	− 5.54
Mg_2SiO_4	7.8[65,66]	4.86[67,68]	3.44[101]	(6.8)	− 8.78	− 0.36	− 5.34
Gd_2SiO_5	6.8[102]	4.9[102]	3.14[103]	6.8	− 8.85	− 1.51	− 5.71
Y_2SiO_5	6.82[102]	4.81[102]	3.24[103]	(6.80)	− 8.78	− 1.41	− 5.54
Al_2O_3	9[44]	(5.7)[44]	3.35[104,105]	(7.06)	− 9.8[44]	− 0.08	− 6.45
$Y_3Al_5O_{12}$	7.1[46]	5.42[46]	3.1[106]	6.77	− 9.38[46]	− 1.71	− 6.28
$BaAl_2O_4$	7.15[107,108,109]	4.63[110,111]	3.41[112]	6.63	− 8.60	− 0.88	− 5.19
$MgAl_2O_4$	6.9[26]	4.4[26]	3.34[113]	(6.8)	− 8.37[26]	− 0.92	− 5.03

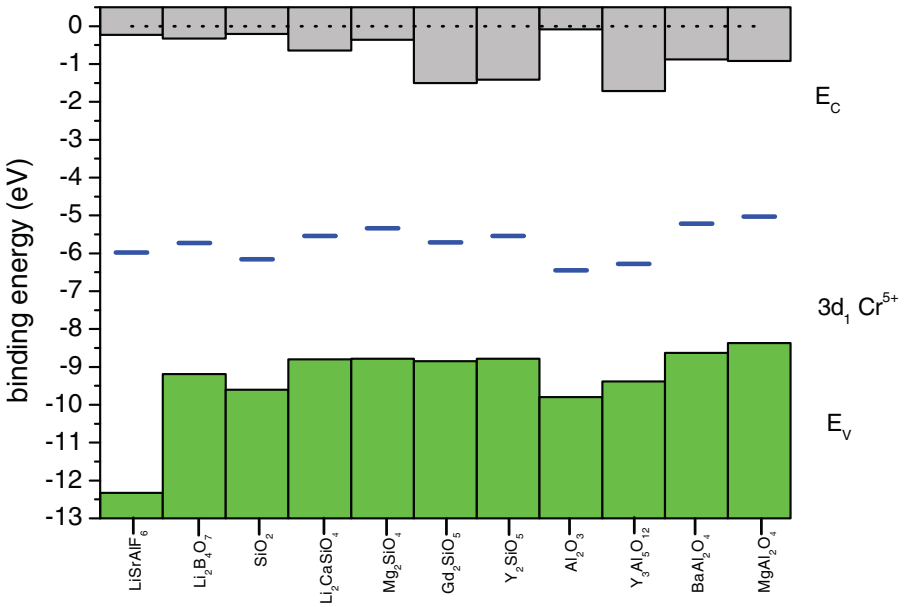

Figure 5. Stacked VRBE schemes for Cr^{6+} doped compounds. The top of the green bars indicate the VRBE E_V at the top of the valence band while the bottom of the gray bars indicate the VRBE E_C at the bottom of the conduction band. Blue horizontal lines denote the VRBE in the Cr^{5+} $E_{3d1}(1, 5+)$ level.

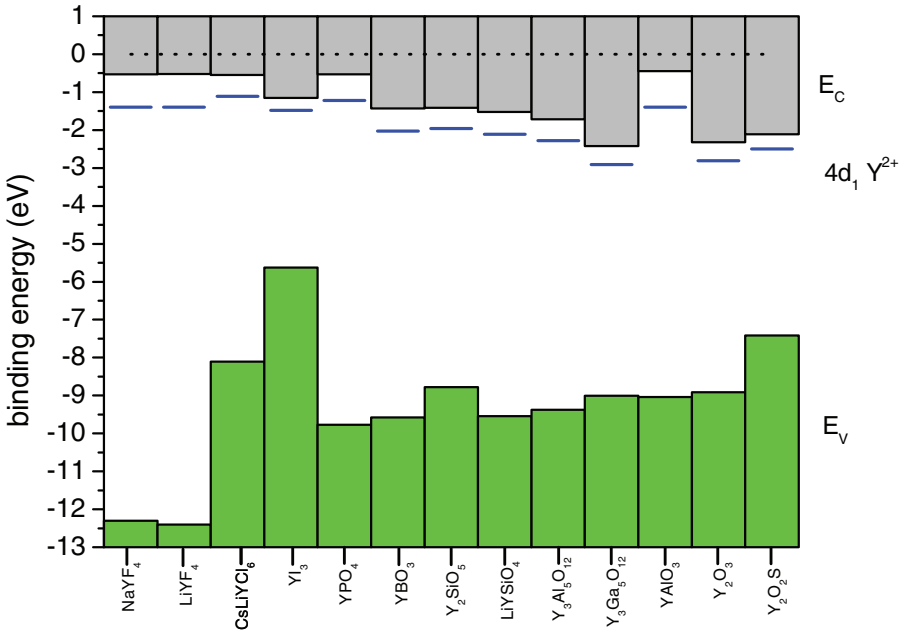

Figure 6. Stacked VRBE schemes Y^{3+} based compounds. The top of the green bars indicate the VRBE E_V at the top of the valence band while the bottom of the gray bars indicate the VRBE E_C at the bottom of the conduction band. Blue horizontal lines denote the VRBE in the Y^{2+} $E_{4d1}(1, 2+)$ level. Data are from Refs. 26, 41, 46, and 114.

Table IV. Experimental, and within brackets estimated or derived, data required for construction of VRBE schemes with the Zr^{3+} $4d^1$ level. All energies are in eV.

Host	E^{ex}	$E^{CT,4f}$	$E^{CT,4d}$	$U(6)$	E_V	E_C	E_{4d_1}
YPO_4	8.55[41]	5.65[41]	7.045[115]	7.09	− 9.77[41]	− 0.54	− 2.72
$LuBO_3$	8.15[41]	5.08[41]	5.61[116]	6.94	− 9.12[41]	− 0.32	− 3.51
SiO_2	8.7[26]	(5.53)[26]	5.98[117]	(7.0)	− 9.6[26]	− 0.36	− 3.62
$Y_3Al_5O_{12}$	7.1[46]	5.42[46]	6.2[118]	6.77	− 9.38[46]	− 1.71	− 3.18
HfO_2	5.85[85]	4.43[85]	5.17[119]	(6.6)	− 8.3[85]	− 1.98	− 3.13
ZrP_2O_7	6.9[70,120]	5.64[121,122]	6.9[70,120]	(7.1)	− 9.7	− 2.55	− 2.8
$MZr_2(PO_4)_3$ (M=Li, Na, K)	6.74[123]	5.96[123]	6.74[123]	(7.1)	− 9.94	− 2.84	− 3.09
$CaZr(PO_4)_2$	6.63[70,124]	5.85[124]	6.63[70,124]	(7.1)	− 9.97	− 2.81	− 3.17
$ZrSiO_4$	6.89[70]	(5.47)[125]	6.89[70]	(6.6)	− 8.6	− 1.25	− 1.5
ZrO_2	5.35[85]	4.43[85]	5.35[85]	(6.6)	− 8.3[85]	− 2.6	− 2.95
$BaZrO_3$	5.4[85]	4.7[85]	5.4[85]	6.55	− 8.55[85]	− 2.8	− 3.15
$SrZrO_3$	5.8[85]	4.2[85]	5.8[85]	6.55	− 8.05[85]	− 1.9	− 2.25
$CaZrO_3$	6.05[85]	4.54[85]	6.05[85]	6.55	− 8.39[85]	− 1.99	− 2.34

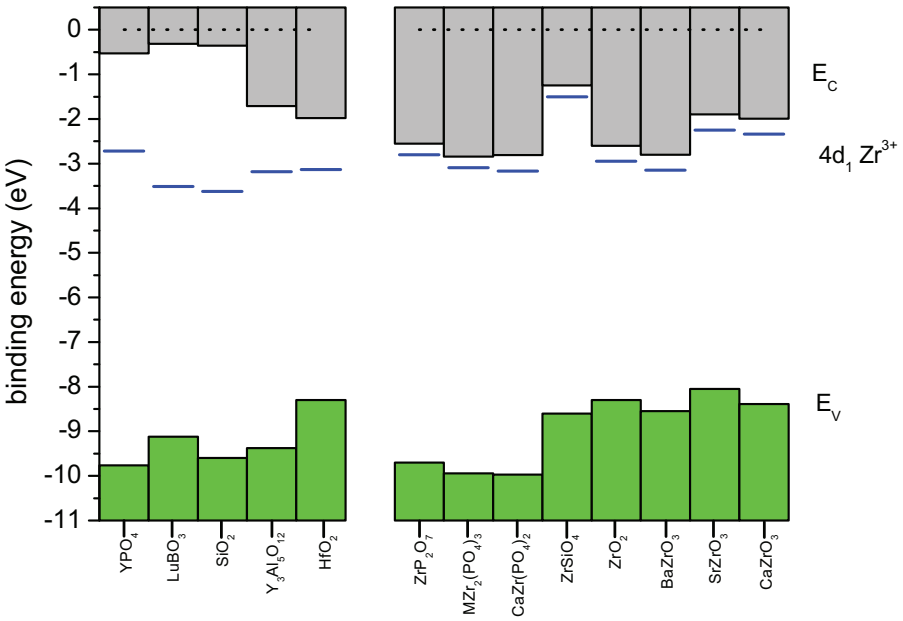

Figure 7. Stacked VRBE schemes for Zr^{4+} doped compounds. The top of the green bars indicate the VRBE E_V at the top of the valence band while the bottom of the gray bars indicate the VRBE E_C at the bottom of the conduction band. Blue horizontal lines denote the VRBE in the Zr^{3+} $E_{4d1}(1, 3+)$ level.

larger than for the analogous 3d TM Ti^{3+}. For yet unknown reasons the VRBE in the Zr^{3+} $4d_1$ level in $ZrSiO_4$ appears much too weak; more and better data is required on this compound to obtain a better estimate.

The next element in the series is Nb^{5+}. The luminescence of niobates and niobium doped rare earth tantalates have been investigated and upon excitation in the ultra-violet (UV) they emit in the blue or near UV parts of the spectrum.[126] Table V compiles the obtained data that was used to create the stacked band scheme of Fig. 8. The average $\overline{E_{4d1}(1, 4+)} = -3.92 \pm 0.09$ eV with approximately 0.7 eV spread.

The final TM of this series is Mo^{6+} which is the 4d analog of the 3d TM Cr^{6+}. In Table VI the obtained data for Mo^{6+} are compiled and displayed as a stacked band scheme in Fig. 9. In the compounds doped with Mo^{6+} an average VRBE $\overline{E_{4d1}(1, 5+)} = -4.78 \pm 0.16$ eV is obtained with a spread of 0.7 eV. The alkaline earth molybdate compounds at the right side of Fig. 8 suggest significantly less bonding in the $4d_1$ level. Most likely the 4d orbital hybridizes with the less strongly bonded alkaline earth related orbitals and then the VRBE of an electron at the bottom of the conduction band and E_X will also rise.

Reviewing the results of this section and comparing them with those of the preceding section, again clear and similar trends emanate. The VRBE of an electron in the lowest energy $4d_1$ level of a TM in different compounds is found at a fairly constant value. The average VRBE becomes stronger (more negative) with higher charge of the TM, and the spread of data around that value, which is mainly attributed to compound to compound variation in crystal field interaction, remains within ±(0.7 to 1) eV. By comparing the VRBE in the $3d_1$ and $4d_1$ levels, as is done in Fig. 1, we observe that the VRBE of a 4d TM is always higher (less negative) than the VRBE of the equivalent 3d TM.

VRBE in the $5d_1$ level of La^{2+}/Eu^{2+}, Ce^{3+}/Hf^{3+}, Ta^{4+} and W^{5+}

The $5d_1$ ground state of La^{2+} and the lowest $5d_1$ excited state of Ce^{3+} are the 5d analogs of the $4d_1$ states of Y^{2+} and Zr^{3+} and of the $3d_1$ states of Sc^{2+} and Ti^{3+}, see Fig. 1. Following the trend in Fig. 1, a progressively weaker bonding of the *n*d-electron is to be expected, and indeed La^{2+} is never encountered in compounds. However there is an abundance of data on Ce^{3+} and Eu^{2+}. In Ref. 27 data were collected on all possible five 4f→5d transition energies for Ce^{3+} in more than 150 host compounds. This provided the centroid shift $\epsilon_c(1, 3+)$ and then with Eq. (2) and Eq. (3), the crucial parameters $U(6)$ and $E_{4f}(7,2+)$ are available. Then automatically $E_{4f}(1, 3+)$ and the sought after $E_{5d1}(1, 3+)$ for Ce^{3+} in these hosts are known.[26] To estimate $E_{5d1}(7, 2+)$ for Eu^{2+} one may use the empirical relationship between the energy $E_{fd1}(7, 2+)$ of the first 4f-5d transition in Eu^{2+} with $E_{fd1}(1, 3+)$ in Ce^{3+}[143]

$$4.22 - E_{fd1}(7, 2+) = 0.64(6.12 - E_{fd1}(1, 3+)) - 0.233eV. \quad [4]$$

The results on all 150 compounds are shown in Fig. 10 where the VRBE $E_{5d1}(1, 3+)$ for Ce^{3+} and $E_{5d1}(7, 2+)$ for Eu^{2+} are given as a function of the coulomb repulsion energy $U(6)$. One observes that

Table V. Experimental, and within brackets estimated or derived, data required for construction of VRBE schemes with the Nb^{4+} $4d^1$ level. All energies are in eV.

Host	E^{ex}	$E^{CT,4f}$	$E^{CT,4d}$	$U(6)$	E_V	E_C	E_{4d_1}
SiO_2	8.7[26]	(5.53)[26]	4.96[117]	(7.0)	− 9.6[26]	− 0.36	− 4.64
$CaTa_2O_6$	4.95[127]	(4.22)[127]	4.35[128]	(6.7)	− 8.14	− 2.94	− 4.24
$YTaO_4$	5.8[28]	5.1[28]	5.17[126]	6.8	− 9.02[28]	− 3.22	− 3.85
$LuTaO_4$	5.8[28]	5.15[28]	4.68[129]	6.8	− 9.07[28]	− 3.27	− 4.39
$ScTaO_4$	5.8[130]	5.2[130]	5.17[128]	6.8	− 9.15[28]	− 3.35	− 3.98
ZrO_2	5.35[85]	4.43[85]	4.13[131]	(6.6)	− 8.3[85]	− 2.6	− 4.17
HfO_2	5.85[85]	4.43[85]	4.61[87]	(6.6)	− 8.3[85]	− 1.98	− 3.69
$LiNbO_3$	4.7[26]	(4.7)[26]	4.7	(6.8)	− 8.67[26]	− 3.59	− 3.97
$CaNb_2O_6$	4.59[132]	(4.33)[132]	4.75	(6.9)	− 8.6[26]	− 3.47	− 3.85
$LaNbO_4$	4.84[79]	(4.49)[80]	4.84	(6.8)	− 8.76[28]	− 3.47	− 3.92
$YNbO_4$	4.9[79]	(4.35)[80]	4.9	(6.8)	− 8.32[28]	− 3.02	− 3.42

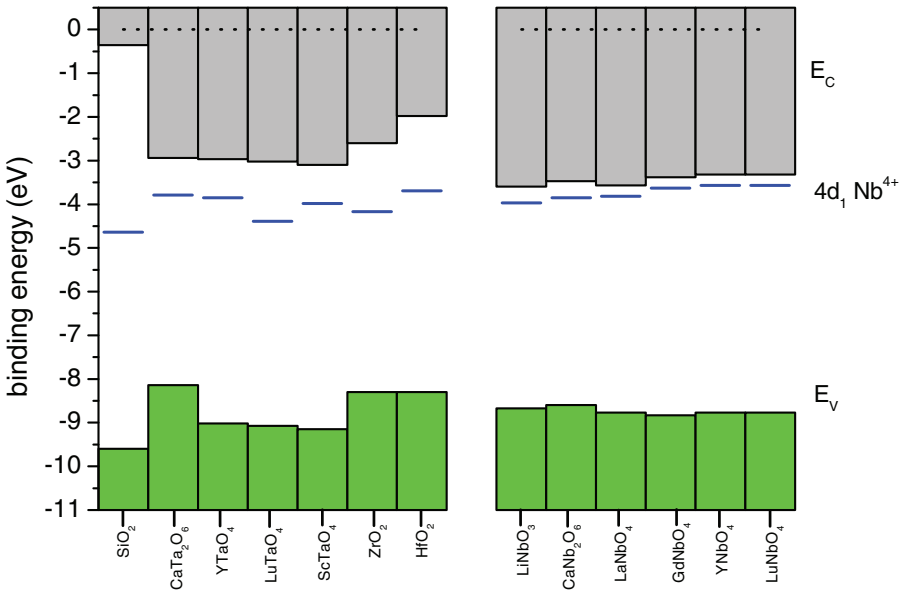

Figure 8. Stacked VRBE schemes for Nb^{5+} doped compounds. The top of the green bars indicate the VRBE E_V at the top of the valence band while the bottom of the gray bars indicate the VRBE E_C at the bottom of the conduction band. Blue horizontal lines denote the VRBE in the Nb^{4+} $E_{4d1}(1, 4+)$ level.

the VRBE $E_{5d1}(1, 3+)$ for Ce^{3+} scatters around a mean value of -1.82 ± 0.02 eV with ± 1.0 eV of scatter. For Eu^{2+} there seems to be a tendency that the VRBE decreases with smaller value for $U(6)$ as indicated by the sloping line through the data. Data scatter ± 0.7 eV around the mean of $\overline{E_{5d1}(7, 2+)} = -0.99 \pm 0.02$ eV. Once the VRBE for the Eu^{2+} electron in the $5d_1$ level is known that for all divalent lanthanides are also known by using the parameters in Ref. 27. One obtains for La^{2+} $\overline{E_{5d1}(1, 2+)} = -0.54$ eV.

The $5d_1$ ground state of Hf^{3+} can like the $5d_1$ excited state of Ce^{3+} also be considered as the 5d analog of the $4d_1$ state of Zr^{3+} or the $3d_1$ state of Ti^{3+}. To estimate $E_{5d1}(1, 3+)$ for Hf^{3+} we will use data on Hf-based compounds from Ref. 85 that are shown in Fig. 11. Like for the Sc-compounds in a preceding section we will assume that the bottom of the conduction band is mainly built from 5d-orbitals. We estimate $E_{5d1}(1, 3+) \approx E_X$ and obtain $\overline{E_{5d1}(1, 3+)} \approx -2.3$ eV.

The next element in our series is the transition metal Ta^{4+}. Spectroscopic information on Ta^{5+} as dopant in four different compounds was found and in addition data on six pure tantalate compounds were used. Data are compiled in Table VII and displayed in Fig. 12. The average $\overline{E_{5d1}(1, 4+)} = -3.25 \pm 0.09$ eV, and data spread $\pm$ 0.5 eV around this mean. The final element in the 5d-series is W^{5+}. Spectroscopic information on W^{6+} as a dopant in a compound was not found and to estimate $\overline{E_{5d1}(1, 5+)}$ we will use VRBE data on the three pure alkaline earth tungstates from Ref. 28 shown in the right hand side of Fig. 11. It suggests $\overline{E_{5d1}(1, 5+)} \approx -3.25$ eV.

Discussion

The average VRBE values $\overline{E_{nd1}(1, Q)}$ for the 3d, 4d, and 5d series of TMs and lanthanides found in this work are displayed in the bottom panel of Fig. 13 against the charge Q. It demonstrates very clear trends. The VRBE becomes more negative within each series by about 1 eV when Q increases by one, and for fixed Q it becomes more negative by 0.5–0.7 eV when the principle quantum number n increaes from 3d to 4d to 5d. The data point for W appears somewhat off placed. Probably, similar to what was observed for the pure alkaline earth molybdates in Fig. 9, there is hybridization between the 5d orbital of W and the less bonded alkaline earth related orbitals leading to an underestimation of the VRBE. The top panel of Fig. 13 shows the 2^{nd}, 3^{rd}, 4^{th} or 5^{th} ionization potentials of the free TMs or lanthanides from Refs. 145–147. The values can be found in the right bottom corners of the elements in the table of Fig. 1 and are equivalent to the $-E_{nd1}(1, Q)$ values for the free ions. The trends for the free ions are very similar to the trends in the bottom panel for the same ions as dopants in compounds. However, the binding energies in the free ion are, depending on the value for Q, 20 to 80 eV stronger. The difference is by definition the chemical shift caused by the coulomb repulsion from the negative ligands around the TM or lanthanide dopant in compounds.

Within the framework of the chemical shift model developed for the 4f-electron VRBE in the lanthanides, the chemical shift $E^{cs}_{nd1}(1, Q)$ can be written as

$$E^{cs}_{nd1}(1, Q) = \frac{-1440Q}{R_Q} eV \quad [5]$$

Table VI. Experimental, and within brackets estimated or derived, data required for construction of VRBE schemes with the Mo^{6+} $4d^1$ level. All energies are in eV.

Host	E^{ex}	$E^{CT,4f}$	$E^{CT,4d}$	$U(6)$	E_V	E_C	E_{4d_1}
SiO_2	8.7[26]	(5.53)[26]	4.35[133,134]	(7.0)	− 9.6[26]	− 0.2	− 5.25
$NaYSiO_4$	(7.45)	5.19[135]	4.25[136]	(6.8)	− 9.16	− 1.11	− 4.91
Al_2O_3	9[44]	(5.7)[44]	4.35[137]	(7.06)	− 9.8[44]	− 0.08	− 5.45
$PbWO_4$	4.35[28]	(4.4)[28]	3.7[138]	7.1	− 8.51[28]	− 3.91	− 4.81
$CaWO_4$	5.25[28]	4.68[28]	4.4[139]	7.1	− 8.8[28]	− 3.3	− 4.4
$LiNbO_3$	4.7[26]	(4.7)[26]	3.68[140]	(6.8)	− 8.67[26]	− 3.59	− 4.99
TiO_2	3.45[63]	3.8[63]	3.44[141]	(6.7)	− 7.72[63]	− 3.99	− 4.28
ZrO_2	5.35[85]	4.43[85]	4.13[142]	(6.6)	− 8.3[85]	− 2.52	− 4.17
$BaMoO_4$	4.9[28]	4.3[28]	4.9	7	− 8.37[28]	− 3.22	− 3.47
$SrMoO_4$	4.9[28]	4.35[28]	4.9	7	− 8.42[28]	− 3.37	− 3.62
$CaMoO_4$	4.6[28]	4.4[28]	4.6	7	− 8.47[28]	− 3.62	− 3.87

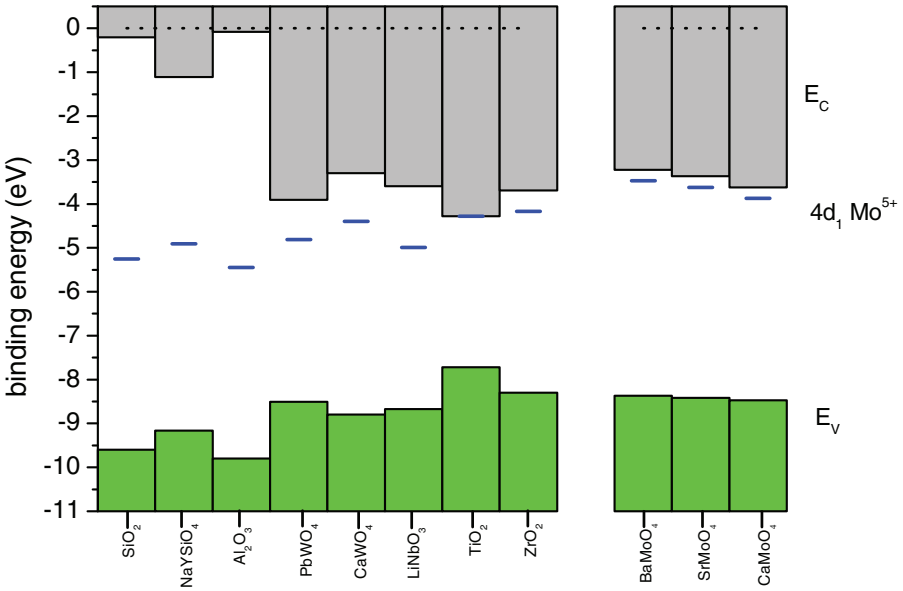

Figure 9. Stacked VRBE schemes for Mo^{6+} doped compounds. The top of the green bars indicate the VRBE E_V at the top of the valence band while the bottom of the gray bars indicate the VRBE E_C at the bottom of the conduction band. Blue horizontal lines denote the VRBE in the Mo^{5+} $E_{4d1}(1, 5+)$ level.

where Q is the charge of the TM or Ln and R_Q the so-called screening distance. The idea is that the charge Q of the TM or Ln is screened by an equal amount of negative charge from the surrounding anion ligands. Eq. (5) then expresses the size of the coulomb repulsion in eV between the *nd* electron and the screening charge located effectively at a distance R_Q expressed in pm. For the 4f-electrons in the lanthanides, the screening distance appeared to be somewhat larger than the Shannon radius of the lanthanide ion. The Shannon radii for the TM cations are given in the left bottom corners of the table in Fig. 1. The radius decreases with higher charge Q and the ratio Q/R_Q in Eq. (5) and the chemical shift will increase accordingly. The results of this work now demonstrate that the almost 70 eV differences in the free ion VRBE values of the *nd* electron is almost fully compensated by the chemical shift resulting in only 5 eV differences in the $\overline{E_{nd1}(1, Q)}$ values. Remarkably, the trends with changing Q and *nd* present in the ionization potentials for the free ions remain present for the ions as dopants in compounds.

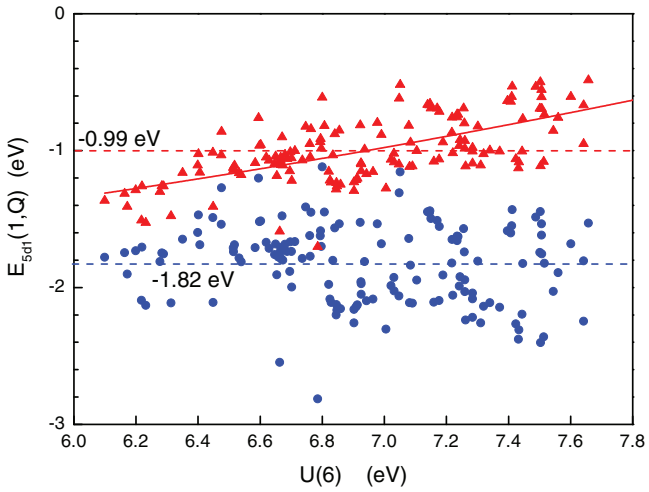

Figure 10. The VRBE $E_{5d1}(1, 3+)$ for the 5d electron in Ce^{3+} (blue circles) and the VRBE $E_{5d1}(1, 2+)$ for the 5d electron in Eu^{2+} (red triangles) as a function of the coulomb repulsion energy $U(6)$. Dashed lines are at the average value. The solid line is to guide the eye in order to indicate a correlation with $U(6)$.

This work has demonstrated that it makes sense to introduce the average VRBE $\overline{E_{nd1}(1, Q)}$ of a single electron in a *nd* impurity state. It implies that as a first approximation the chemical shift of the binding energy from the free ion value to the in-compound value for a particular TM is about the same in all compounds. The same conclusion was made for the VRBE of 4f electrons in the lanthanides. However, individual data on $E_{nd1}(1, Q)$ scatter more strongly around the average than what is observed for 4f-electron binding energies. Partly this will be caused by errors in the values for E_V and $E^{CT,nd}$ that may add up to an estimated 0.5 eV error in $E_{nd1}(1, Q)$, and when better data are available this error may be reduced. However we believe that the main reason is that the *nd* electron has a much stronger interaction with the surrounding anion ligands than the well shielded $4f$ electron. It leads to a 2–3 eV large crystal field splitting of the *nd* level energies, see for example the compilation of data on crystal field splitting in Refs. 148 and 149. The scatter of data in $E_{5d1}(1, 3+)$ for Ce^{3+} as shown in Fig. 10 is for example almost entirely due to from compound to compound variation in crystal field splitting. Covalence between the *nd*-orbital and anion ligands leads to additional bonding of the *n*d-electron and may thus lower $E_{nd1}(1, Q)$. This is most likely the cause of the apparent reduction of $E_{5d1}(1, 2+)$ for Eu^{2+} in Fig. 10 with smaller value of $U(6)$ and is closely related to the nephelauxetic effect. Although such detailed information is not available on the 4*d* and 3*d* ions in this work, it seems likely that covalency or the nepehelauxetic effect has also its contribution to $E_{nd1}(1, Q)$. A full analysis of these effects would require detailed computational work that is currently beyond the scope of this investigation. Note that in our methods we always assumed that the energy of electron transfer from the valence band into the empty *nd* level of the TM^Q provides a good measure for the level location of the lowest nd_1 level of the TM^{Q-1} above the valence band. This is a well established method to place the Eu^{2+} 4f ground state level above the valence band. However, this is not yet established for the TMs studied in this work, and systematic error of yet unkown magnitude can or will be present in the obtained $\overline{E_{nd1}(1, Q)}$ values. For example, in the case of Ce^{4+} it was found that the onset energy of electron transfer from the valence band to the empty 4f-orbital provides a better measure for the location of the Ce^{3+} 4f ground state level above E_V than the energy at the maximum of the CT-band.[41] Independent methods are required to establish the size of such systematic error for the TMs. With techniques like thermoluminescence studies or photocurrent experiments one might determine, for example, how deep an electron in the TM^{Q-1} nd_1 level is below the conduction band.

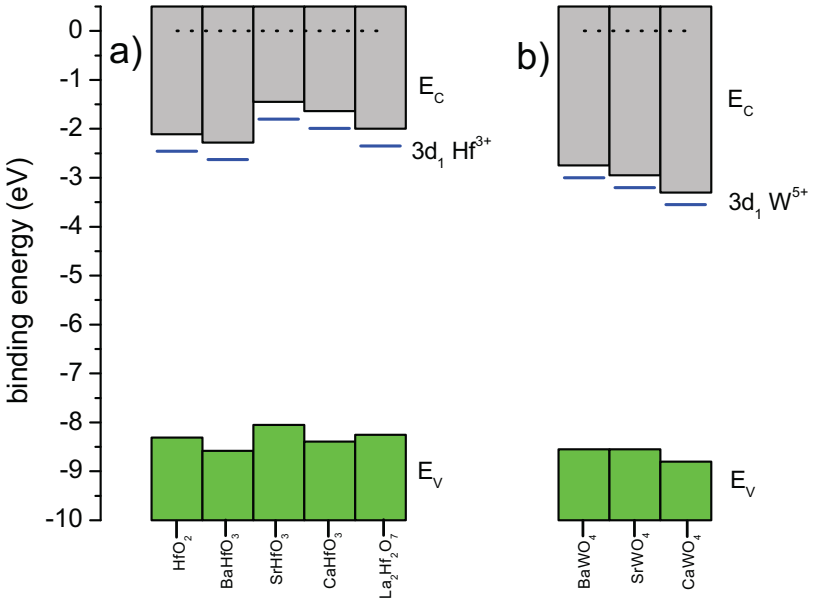

Figure 11. Stacked VRBE schemes for a) Hf^{4+} and b) W^{6+} based compounds. The top of the green bars indicate the VRBE E_V at the top of the valence band while the bottom of the gray bars indicate the VRBE E_C at the bottom of the conduction band. Blue horizontal lines denote the VRBE in the Hf^{3+} $E_{5d1}(1, 3+)$ or W^{5+} $E_{5d1}(1, 3+)$ level. Hf data are from Ref. 85 and W data are from Ref. 28.

Table VII. Experimental, and within brackets estimated or derived, data required for construction of VRBE schemes with the Ta^{5+} $5d^1$ level. All energies are in eV.

Host	E^{ex}	$E^{CT,4f}$	$E^{CT,4d}$	U	E_V	E_C	E_{5d_1}
SiO_2	8.7[26]	(5.53)[26]	5.34[117]	(7.0)	− 9.6	− 0.2	− 4.43
$LaTaO_4$	5.1[28]	4.41[28]	5.1[28]	6.7	− 8.47[28]	− 3.12	− 3.37
$GdTaO_4$	5.8[28]	5[28]	5.8[28]	6.7	− 8.92[28]	− 2.87	− 3.12
$YTaO_4$	5.8[28]	5.1[28]	5.8[28]	6.7	− 9.02[28]	− 2.97	− 3.22
$LuTaO_4$	5.8[28]	5.15[28]	5.8[28]	6.7	− 9.07[28]	− 3.02	− 3.27
$ScTaO_4$	5.8[28]	5.2[28]	5.8[28]	6.7	− 9.15[28]	− 3.1	− 3.35
$CaTa_2O_6$	4.95[127]	(4.22)[127]	4.95[127]	(6.7)	− 8.14	− 2.94	− 3.19
ZrO_2	5.35[85]	4.43[85]	5.17[131]	(6.6)	− 8.3	− 2.6	− 3.13
BaZrO3	5.4[85]	4.7[85]	4.77[144]	6.55	− 8.55	− 2.8	− 3.78
HfO_2	5.85[85]	4.43[85]	5.51[87]	(6.6)	− 8.3	− 1.98	− 2.79

Despite unknown error margins, the value of this work is that we have obtained a first indication on where to expect the electron acceptor state of transition metals with empty *nd*-orbital or equivalently the electron donor state of transition metals with a single electron in the *nd*-orbital. When data are also available on E_C or E_V of the host compound one may better understand or even predict the luminescence, electron donating, or electron accepting properties of TM doped compounds because often those properties are connected with the relative positions of impurity states with respect to the host band states. Since the VRBE of the lanthanide 4f levels are

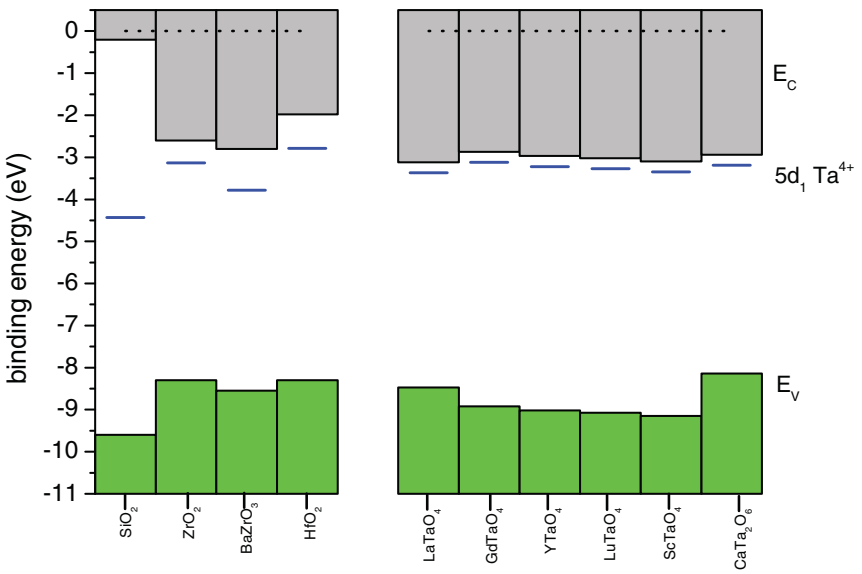

Figure 12. Stacked VRBE schemes for Ta^{5+} doped compounds. The top of the green bars indicate the VRBE E_V at the top of the valence band while the bottom of the gray bars indicate the VRBE E_C at the bottom of the conduction band. Blue horizontal lines denote the VRBE in the Ta^{4+} $E_{5d1}(1, 3+)$ level.

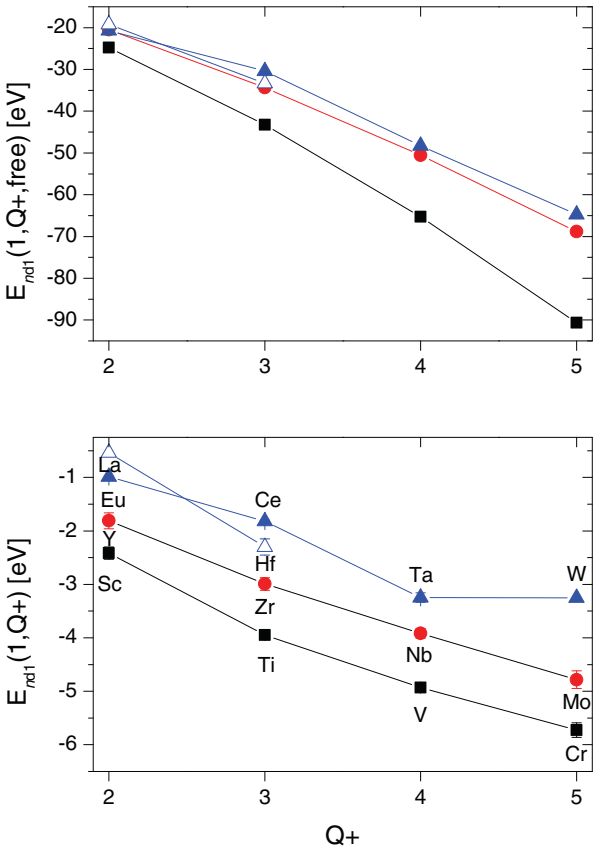

Figure 13. Comparison of $E_{nd1}(1, Q)$ for the free ion (top panel) with the average $E_{nd1}(1, Q)$ in compounds (bottom panel) for n=3 (black square), 4 (red circle) or 5 (blue triangle).

well established, similar knowledge on the *nd*-levels enables one to much better understand the interplay between a TM and lanthanide impurity. For example the VRBE of the 4f-electron in the ground state of Eu^{2+} is always near −4 eV. It implies that V^{5+} will oxidize Eu^{2+} to form Eu^{3+} and V^{4+} with $E_{3d1}(1, 4+) \approx -5$ eV. The finding that the VRBE of an electron in the lowest 5d-level of Ce^{3+} is on average above that of the lowest 5d-level of Hf^{3+} implies that the emitting 5d-level of Ce^{3+} tends to be located above E_X in Hf^{4+} based compounds. Ce^{3+} 5d-4f emission cannot be observed under such conditions.

Conclusions

Data were collected on the energy of electron transfer from the valence band to the empty *nd* orbital of 3d, 4d, and 5d transition metal and lanthanide impurities in compounds. The chemical shift model developed for lanthanide doped compounds was used to determine the VRBE at the top of the valence band, and combined this gives the VRBE of the electron in the lowest nd_1 level of the TM or Ln impurity. The VRBE in the lowest nd_1 state of a TM or Ln remains fairly constant from compound to compound and it made sense to define the average VRBE $\overline{E_{nd1}(1, Q)}$ as compiled in Fig. 1 and displayed in Fig. 13. It increases (becomes more negative) with higher charge of the TM or Ln. Bonding is strongest in the 3d-orbital and weakens for 4d and further for 5d-orbitals. These trends follow the known trends for the free ion ionization potentials. The compound to compound spread in $E_{nd1}(1, Q)$ around the mean value is for all TM and lanthanides of the order of ±(0.7–1) eV and is mainly atributed to compound to compound variation in the crystal field splitting of the *nd* levels.

Appendix A

Below an account is given on how data of some of the compounds in the tables of this work were obtained. One may estimate the value for $U(6)$ for a compound by comparison with known values for other related compounds, and then the VRBE of the electron in the ground state of Eu^{2+} can be calculated with the chemical shift model. ±0.1 eV error in $U(6)$ creates about ± 0.05 eV error in $E_{4f}(7, 2+)$ which is good enough for the purpose of this work. If available the energy of the CT band of Eu^{3+} will be used to obtain E_V. For some compounds Pr^{3+} or Tb^{3+} IVCT data are known that can be used to place the bottom of the conduction band at E_C. Knowledge on E^{ex}, that will always be specified for temperature around 10K, then provides either E_C or E_V.

$LiSrAlF_6$ For $U(6)$ a value of 7.69 eV was used. It is based on $U(6) = 7.64$ eV in Ref. 27 for the related compound $LiCaAlF_6$. The value is estimated 0.05 eV larger because, when other properties remain the same, U tends to increase with larger site size. $E^{ex}(LT) = 11.2$ eV is from Refs. 88–90. Ref. 91 observes the Eu^{3+} CT-band at 7.9 eV.

$CaSO_4$ $U(6) = 7.19$ eV is estimated from the centroid shift of the Ce^{3+} 5d-levels[27] and $E^{ex}(LT) = 8.45$ eV is derived from Refs. 52, 53. E^{CT} for Eu^{3+} is at 4.77 eV from Refs. 54 and 55.

ZrP_2O_7 For $U(6)$ a value of 7.1 eV will be used that is typical for pyrosilicate compounds. The host excitation maximum is not yet well established. $E^{ex}(RT)$ is at 7.0 eV in Ref. 70 but $E^{ex}(8K) = 6.71$ eV in Ref. 120. Our best estimate is then $Eex(LT) = 6.9 \pm 0.2$ eV. The charge transfer band is at 5.6 eV or higher energy[122] which yields $E_V \approx -9.7$ eV or even lower.

$MZr_2(PO_4)_3$ (M=Li, Na, K) All three compounds have very similar spectroscopic properties so their related electronic structures are similar too. For $U(6)$ a value of 7.1 eV will be used. The room temperature host excitation maximum is at 6.74 eV in Ref. 123 from which $E^{ex}(LT)$ of 6.85 eV is estimated. The Eu^{3+} CT-band is at 213 nm (5.82 eV)[123] which then yields $E_V = -9.94$ eV.

$CaZr(PO_4)_2$ Similar to other phosphate compounds $U(6)$ is estimated to be near 7.1 eV. The room temperature host excitation maximum is observed at 184 nm and 187 nm in Ref. 124 from which $E^{ex}(LT)$ of 6.80 eV is estimated. The Eu^{3+} CT band is at 212 nm (5.85 eV) which then yields $E_V = -9.97$ eV.

$Li_2B_4O_7$ Ccondensed borates like SrB_4O_7 and $CaLaB_7O_{13}$ have values for $U(6)$ near 7.2 eV,[27] so the same value was used for $Li_2B_4O_7$. $E^{ex}(LT) = 8.2$ eV is obtained from studies in Ref. 93 on a pure sample. Eu^{3+} on a much smaller Li^+ site in crystalline $Li_2B_4O_7$ will create a large lattice distortion and furthermore requires charge compensation. Data on the CT energy was not found and here we will use for E^{CT} a value of 5.04 eV from Ref. 94 that was observed for glassy $Li_2B_4O_7$.

$GdAl_3(BO_3)_4$ $U(6) = 7.02$ eV is estimated from the centroid shift of the Ce^{3+} 5d levels in Ref. 27. The room temperature exciton creation peak is consistently reported at 7.45 eV[29–31] and we will assume for $E^{ex}(LT)$ a value of 7.55 eV. The maximum of the Eu^{3+} CT band is reported in several papers to be between 249 nm and 256 nm[30–34] and here we will adopt $E^{CT} = 4.90$ eV.

$YAl_3(BO_3)_4$ $U(6) = 7.03$ eV is estimated from the centroid shift of the Ce^{3+} 5d levelsin.[27] From Refs. 29, 30, 36, and 37 the low temperature exciton creation peak is at $E^{ex}(LT) = 7.65$ eV . The maximum of the Eu^{3+} CT band is near 241 nm (5.15 eV) as reported in Refs. 36, 38, and 39.

GeO_2 An $E^{ex}(LT)$ of about 5.9 eV is derived from the fundamental absorption threshold near 5.6 eV in Ref. 61, the first reflection peak at 5.82 eV in Ref. 150, the bandgap at 5.7+/−0.1 eV in Ref. 151 and at 5.81 eV in Ref. 152. There are no lanthanide spectroscopic data available to apply the chemical shift model. Instead we will use information on the valence band offset at the interface between a thin film of GeO_2 and Ge. A value of 4.0 eV is reported in Ref. 151 and 4.5 eV in Ref. 152. In Ref. 152 uses a band bending of 0.6 eV at the Ge-GeO_2 interface and then by using that $E_V(Ge) = -4.8$ eV from the photoelectron threshold in Ref. 153 one obtains $E_V(GeO_2) = -8.7$ eV.

$ZrSiO_4$ For $U(6)$ a value of 6.9 eV, similar to Li_2CaSiO_4 (see below), was used. $E^{ex}(LT) = 7.1$ eV is estimated from Ref. 70. The energy of the Eu^{3+} CT-band is uncertain because it is reported at 268 nm (4.63 eV) in Ref. 71 and at 304 nm (4.08 eV) in Ref. 154. It leads to $E_V = -8.65$ eV or −8.05 eV. The first value agrees well with $E_V = -8.55$ eV proposed by Ref. 155.

Li_2CaSiO_4 From the centroid shift of the Ce^{3+} 5d levels $U(6) = 6.92$ eV is estimated in Ref. 27, $E^{ex}(LT) = 7.55$ eV is from Ref. 97. The CT-band energy for Eu^{3+} is reported at 4.77 eV in Ref. 98 and 99 for 0.5% and 10% Eu^{3+} doping concentration.

Mg_2SiO_4 For Mg_2SiO_4 a value of $U(6)$ of 6.8 eV has been used. We will use $E^{ex}(LT) = 7.8$ eV which is based on the fundamental absorption onset at 7.56 eV in Ref. 65 and the excitation maximum of intrinsic luminescence near 7.8 eV in Ref. 66. Excitation spectra shows the Eu^{3+} CT band at 254nm in Ref. 67 and at 256 nm in Ref. 68 corresponding to $E^{CT} = 4.86$ eV.

$NaYSiO_4$ Like for other orthosilicates $U(6) = 6.8$ eV is estimated. Information on E^{ex} was not found and we will use 7.45 eV which is the same value as for $LiYSiO_4$ in Ref. 156 and 135 reports the CT-band at 239 nm (5.19 eV) but Ref. 136 reports 275 nm (4.51 eV) for a sample containing 30% Eu^{3+}. We will tentatively adopt the value of 5.19 eV which then yields $E_V = -9.16$ eV.

Gd_2SiO_5 The electronic properties of Gd_2SiO_5 are expected to be quite similar to those of Lu_2SiO_5 where $U(6) = 6.8$ eV.[27] $E^{ex}(LT)$ has a well established value of 6.80 eV from Refs. 157 and 158 and is practically same as in Y_2SiO_5 and Lu_2SiO_5.

The maximum of the Eu^{3+} CT-band is reliably established at 252 nm (4.90 eV) from Refs. 157 and 158.

X2-Y_2SiO_5 The electronic properties of Y_2SiO_5 are quite similar to those of Lu_2SiO_5 where $U(6) = 6.8$ eV.[27] $E^{ex}(LT) = 6.82$ eV from Refs. 159 and 160. For the X2 crystallographic phase E^{CT} is near 4.8 eV as reported in Refs. 161–163. For the X1 crystallographic phase the CT energy is reported near 5.1 eV in Refs. 164 and 165. Photocurrent studies in Ref. 166 show that the first two 5d bands of Ce^{3+} are below the conduction band bottom.

CaYAlO$_4$ From the centroid shift in Ref. 27 a value of 6.7 eV is estimated which will be used in this work. From $E^{ex}(RT)$ at 210 nm (5.9 eV) in Ref. 75 $E^{ex}(LT)$ is estimated at 6.0 eV. The Eu^{3+} charge transfer band is at 272 nm (4.56 eV) in Ref. 167 and 240 nm (5.17 eV) in Ref. 75 yielding a still uncertain value of -8.6 ± 0.3 eV for E_V.

$BaAl_2O_4$ $U(6)$ is estimated to be similar to other aluminates like $YAlO_3$ and $Y_3Al_5O_{12}$ and a value of 6.8 eV is adopted. From Refs. 107–109 $E^{ex}(LT)$ is estimated at 7.15 eV. The Eu^{3+} charge transfer band is at 263 nm (4.71 eV) in Ref. 110 and at 273 nm (4.54 eV) in Ref. 111. An average value of E^{CT} of 4.63 eV was used, leading to a value of -8.6 eV for E_V.

$CaTa_2O_6$. As for other tantalate compounds in Ref. 28 we will use $U(6) = 6.7$ eV. The excitation spectrum for Pr^{3+} luminescence in Ref. 127 shows an excitation band at 256 nm that was attributed to the host excitation from which $E^{ex}(LT)$ of 4.95 eV is estimated. A shoulder band near 298 nm (4.16 eV) was attributed to the Pr^{3+} IVCT band from which $E_V = -8.14$ eV is obtained. Upon excitation both blue emissions from the $^3P_0$ and red emissions from the $^1D_2$ level are observed; the blue emission is brightest.

References

1. P. F. Smet, A. B. Parmentier, and D. Poelman, *Journal of The Electrochemical Society*, **158**, R37 (2011).
2. A. Zukauskas, R. Vaicekauskas, P. Vitta, A. Zabiliute, A. Petrulis, and M. Shur, *Optics Express*, **21**, 26642 (2013).
3. N. C. George, K. A. Denault, and R. Seshadri, *Annual Review of Materials Research*, **43**, 481 (2013).
4. R.-J. Xie, N. Hirosaki, T. Takeda, and T. Suehiro, *ECS Journal of Solid State Science and Technology*, **2**, R3031 (2013).
5. O. M. ten Kate, M. de Jong, H. T. Hintzen, and E. van der Kolk, *Journal of Applied Physics*, **114**, (2013).
6. W. G. J. H. M. van Sark, J. de Wild, J. K. Rath, A. Meijerink, and R. E. I. Schropp, *Nanoscale Research Letters*, **8**, 1 (2013).
7. D. Verma, T. O. Saetre, and O. M. Midtgard, in *Photovoltaic Specialists Conference (PVSC), 2012 38th IEEE* (2013), pp. 002608–002613.
8. K. Van den Eeckhout, D. Poelman, and P. Smet, *Materials*, **6**, 2789 (2013).
9. H. F. Brito, J. Hls, T. Laamanen, M. Lastusaari, M. Malkamaki, and L. C. V. Rodrigues, *Optical Materials Express*, **2**, 371 (2012).
10. P. F. Smet, D. Poelman, and M. P. Hehlen, *Optical Materials Express*, **2**, 452 (2012).
11. P. Lecoq, A. Annenkov, A. Gektin, M. Korzhik, and C. Pedrini, *How User's Requirements Influence the Development of a Scintillator* (Springer Berlin Heidelberg, 2006), chap. 2, pp. 35–80, Particle Acceleration and Detection.
12. G. Bizarri, *Journal of Crystal Growth*, **312**, 1213 (2010).
13. C.-D. Lee, T. Hartnett, and R. Tustison (2012), vol. **8373**, pp. 83730X–83730X–6.
14. R. W. Novotny, *Nuclear Physics News*, **20**, 27 (2010).
15. R. Stone, *Science*, **325**, 1336 (2009).
16. E. Nakamura and K. Sato, *Nat Mater*, **10**, 158(2011).
17. M. A. de Boer and K. Lammertsma, *ChemSusChem*, **6**, 2045 (2013).
18. T. E. Graedel, E. M. Harper, N. T. Nassar, and B. K. Reck, *Proceedings of the National Academy of Sciences* (2013).
19. A. Canning, A. Chaudhry, R. Boutchko, and N. Gronbech-Jensen, *Physical Review B*, **83**, 125115 (2011).
20. P. Dorenbos, *Physical Review B*, **85**, 165107 (2012).
21. L. Petit, R. Tyer, Z. Szotek, W. M. Temmerman, and A. Svane, *New Journal of Physics*, **12**, 113041 (2010).
22. Y. Xu and M. A. A. Schoonen, *American Mineralogist*, **85**, 543 (2000).
23. E. Rogers, P. Dorenbos, and E. van der Kolk, *New Journal of Physics*, **13**, 93038 (2011).
24. R. D. Shannon, *Acta Crystallographica A*, **32**, 751 (1976).
25. P. Dorenbos, *Journal of Physics: Condensed Matter*, **15**, 4797 (2003).
26. E. G. Rogers and P. Dorenbos, *Journal of Luminescence*, **153**, 40 (2014).
27. P. Dorenbos, *Journal of Luminescence*, **135**, 93 (2013).
28. P. Dorenbos and E. G. Rogers, *ECS Journal of Solid State Science and Technology*, **3**, R150 (2014).
29. O. Aloui-Lebbou, C. Goutaudier, S. Kubota, C. Dujardin, M. T. Cohen-Adad, C. Pedrini, P. Florian, and D. Massiot, *Optical Materials*, **16**, 77 (2001).
30. Y. Hongpeng, G. Hong, X. Zeng, C. H. Kim, C. H. Pyun, B. Y. Yu, and H. S. Bae, *Journal of Physics and Chemistry of Solids*, **61**, 1985 (2000).
31. Y. H. Wang and X. X. Li, *Journal of The Electrochemical Society*, **153**, G238 (2006).
32. W. Park, R. Y. Lee, C. J. Summers, Y. R. Do, and H. G. Yang, *Materials Science and Engineering: B*, **78**, 28 (2000).
33. L. S. Wang, X. M. Liu, Z. W. Quan, D. Y. Kong, J. Yang, and J. Lin, *Journal of Luminescence*, **122–123**, 36(2007).
34. X. X. Li, Y. H. Wang, Y. Hao, and L. L. Wang, *Journal of The Electrochemical Society*, **153**, G807 (2006).
35. X. X. Li, Z. Chen, and Y. H. Wang, *Journal of Alloys and Compounds*, **472**, 521(2009).
36. N. Yokosawa, K. Suzuki, and E. Nakazawa, *Japanese Journal of Applied Physics*, **42**, 5656 (2003).
37. V. P. Dotsenko, I. V. Berezovskaya, N. P. Efryushina, A. S. Voloshinovskii, and G. B. Stryganyuk, *Journal of Materials Science*, **45**, 1469 (2010).
38. L. Wang, Y. Wang, and H. Gao, *Journal of The Electrochemical Society*, **153**, G943 (2006).
39. K.-G. Lee, B.-Y. Yu, C.-H. Pyun, and S.-I. Mho, *Solid State Communications*, **122**, 485 (2002).
40. H. Yoshida, K. Fujikawa, H. Toyoshima, S. Watanabe, and K. Ogasawara, *Physica Status Solidi (a)*, **203**, 2701 (2006).
41. P. Dorenbos, *Journal of Physics: Condensed Matter*, **25**, 225501(2013).
42. L. Wang and Y. Wang, *Journal of Luminescence*, **122 to 123**, 921 (2007).
43. Y. Wu, G. Ren, M. Nikl, D. Ding, J. Wang, S. Shang, F. Yang, and S. Pan, *The Journal of Physical Chemistry A*, **115**, 13821 (2011).
44. P. Dorenbos, *Physical Review B*, **87**, 035118 (2013).
45. M. Kirm, G. Zimmerer, E. Feldbach, A. Lushchik, C. Lushchik, and F. Savikhin, *Physical Review B*, **60**, 502 (1999).
46. P. Dorenbos, *Journal of Luminescence*, **134**, 310 (2013).
47. V. Murk and N. Yaroshevich, *Physica Status Solidi (b)*, **181**, K37 (1994).
48. Y. Zorenko, V. Gorbenko, T. Voznyak, T. Zorenko, M. Nikl, and K. Nejezchleb, *Journal of Luminescence*, **128**, 595 (2008).
49. Y. V. Zorenko, *Optics and Spectroscopy*, **100**, 572 (2006).
50. N. N. Ryskin, P. Dorenbos, C. W. E. van Eijk, and S. K. Batygov, *Journal of Physics: Condensed Matter*, **6**, 10423(1994).
51. J.-G. Li and T. Ishigaki, *Journal of Solid State Chemistry*, **196**, 58 (2012).
52. E. van der Kolk, P. Dorenbos, A. P. Vink, R. C. Perego, C. W. E. van Eijk, and A. R. Lakshmanan, *Physical Review B*, **64**, 195129(2001).
53. A. R. Lakshmanan, S. B. Kim, H. M. Jang, B. G. Kum, B. K. Kang, S. Heo, and D. Seo, *Advanced Functional Materials*, **17**, 212 (2007).
54. D. van der Voort and G. Blasse, *Journal of Solid State Chemistry*, **87**, 350 (1990).
55. A. Lakshmanan, S.-B. Kim, B. G. Kum, H. M. Jang, and B. K. Kang, *physica status solidi (a)*, **203**, 565 (2006).
56. G. Blasse and G. P. M. Van Den Heuvel, *Journal of Solid State Chemistry*, **15**, 289 (1975).
57. K. S. Shim, Y. R. Jung, B. K. Moon, B. C. Choi, J. H. Jeong, J. S. Bae, and J. H. Kim, *Journal of the Korean Physical Society*, **53**, 3568 (2008).
58. C. Li, Z. Hou, C. Zhang, P. Yang, G. Li, Z. Xu, Y. Fan, and J. Lin, *Chemistry of Materials*, **21**, 4598 (2009).
59. M. A. Aia, *Journal of The Electrochemical Society*, **114**, 367 (1967).
60. M. F. Hazenkamp and G. Blasse, *The Journal of Physical Chemistry*, **96**, 3442 (1992).
61. H. A. Papazian, *Journal of Applied Physics*, **27**, 1253 (1956).
62. D. P. Madacsi, L. A. Kappers, and J. F. Houlihan, *Physica Status Solidi (b)*, **91**, K105 (1979).
63. P. Dorenbos, *ECS Journal of Solid State Science and Technology*, **3**, R19(2014).
64. K. Fujiyoshi, H. Yokoyama, F. Ren, and S. Ishida, *Journal of the American Ceramic Society*, **76**, 981 (1993).
65. C.-H. Kim, I.-E. Kwon, C.-H. Park, Y.-J. Hwang, H.-S. Bae, B.-Y. Yu, C.-H. Pyun, and G.-Y. Hong, *Journal of Alloys and Compounds*, **311**, 33 (2000).
66. M. Kitaura and A. Ohnishi, *physica status solidi (c)*, **6**, 236 (2009).
67. H. Yang, J. Shi, M. Gong, and K. W. Cheah, *Journal of Luminescence*, **118**, 257 (2006).
68. S. C. Prashantha, B. N. Lakshminarasappa, and B. M. Nagabhushana, *Journal of Alloys and Compounds*, **509**, 10185(2011).
69. T. C. Brunold, H. U. Gudel, and A. A. Kaminskii, *Chemical Physics Letters*, **271**, 327 (1997).
70. M. Kaneyoshi, *Journal of Luminescence*, **121**, 102 (2006).
71. M. Gaft, G. Panczer, R. Reisfeld, I. Shinno, B. Champagnon, and G. Boulon, *Journal of Luminescence*, **87–89**, 1032(2000).
72. A. Niesert, R. Sievers, A. Siggel, K. Langer, and M. Jansen, *Solid State Sciences*, **6**, 1149 (2004).
73. A. Suchocki, A. Brenier, C. Pedrini, and G. Boulon, *Journal de physique IV*, **01**, C7 (1991).
74. G. Jia, P. A. Tanner, and B.-M. Cheng, *Chemical Physics Letters*, **474**, 97 (2009).
75. M. Bartic, H. Kominami, Y. Nakanishi, and K. Hara, *Optical properties of CaYAlO(4):Eu(3+) phosphors* (Trans Tech Publications Ltd, Stafa-Zurich, 2011), Vol. 222 of Advanced Materials Research, pp. 231–234.
76. M. Yamaga, T. Yosida, Y. Inoue, N. Kodama, and B. Henderson, *Radiation Effects and Defects in Solids*, **136**, 33 (1995).
77. Y. Fujimoto, H. Tanno, K. Izumi, S. Yoshida, S. Miyazaki, M. Shirai, K. Tanaka, Y. Kawabe, and E. Hanamura, *Journal of Luminescence*, **128**, 282 (2008).
78. Y. Dong, S. Liu, W. Li, Y. Kong, S. Chen, and J. Xu, *Opt. Lett.*, **36**, 1779(2011).
79. A. H. Krumpel, P. Boutinaud, E. van der Kolk, and P. Dorenbos, *Journal of Luminescence*, **130**, 1357 (2010).
80. P. Boutinaud, E. Pinel, M. Oubaha, R. Mahiou, E. Cavalli, and M. Bettinelli, *Optical Materials*, **28**, 9 (2006).
81. L. Zhou, J. Huang, F. Gong, Y. Lan, Z. Tong, and J. Sun, *Journal of Alloys and Compounds*, **495**, 268 (2010).
82. S. Klosek and D. Raftery, *The Journal of Physical Chemistry B*, **105**, 2815 (2001).
83. K. W. Blazey, M. Aguilar, J. G. Bednorz, and K. A. Mller, *Physical Review B*, **27**, 5836 (1983).
84. C. Gargori, S. Cerro, R. Galindo, A. Garcia, M. Llusar, J. Badenes, and G. Monros, *Ceramics International*, **37**, 3665 (2011).
85. P. Dorenbos, *Journal of Luminescence*, **151**, 224 (2014).

86. F. Ren, S. Ishida, and N. Takeuchi, *Journal of the American Ceramic Society*, **76**, 1825 (1993).
87. A. Wiatrowska and E. Zych, *The Journal of Physical Chemistry C*, **116**, 6409 (2012).
88. M. Henke, *Ph.D. thesis*: Interkonfigurale Übergänge Lanthanid-dotierter Kristalle, Hamburg University, Germany (2001).
89. K. Shimamura, H. Sato, A. Bensalah, V. Sudesh, H. Machida, N. Sarukura, and T. Fukuda, *Crystal Research and Technology*, **36**, 801 (2001).
90. M. True, M. Kirm, E. Negodine, S. Vielhauer, and G. Zimmerer, *Journal of Alloys and Compounds*, **374**, 36 (2004).
91. M. Kirm, Y. Chen, S. Neicheva, K. Shimamura, N. Shiran, M. True, and S. Vielhauer, *physica status solidi (c)*, **2**, 418 (2005).
92. H. von Lips, N. Schwentner, G. Sliwinski, and K. Petermann, *Journal of Applied Spectroscopy*, **62**, 803 (1995).
93. I. N. Ogorodnikov, V. A. Pustovarov, A. V. Kruzhalov, L. I. Isaenko, M. Kirm, and G. Zimmerer, *Physics of the Solid State*, **42**, 464 (2000).
94. M. Ignatovych, V. Holovey, A. Watterich, T. Vidoczy, P. Baranyai, A. Kelemen, V. Ogenko, and O. Chuiko, *Radiation Physics and Chemistry*, **67**, 587 (2003).
95. S. M. Kaczmarek, C. Koepke, M. Grinberg, A. Majchrowski, K. Wisniewski, and M. Czuba, *Proc. SPIE*, **4412**, 389 (2001).
96. C. Koepke, K. Wisniewski, M. Grinberg, and F. Rozploch, *Journal of Physics-Condensed Matter*, **14**, 11553 (2002).
97. P. Dorenbos, L. Pierron, L. Dinca, C. W. E. van Eijk, A. Kahn-Harari, and B. Viana, *Journal of Physics-Condensed Matter*, **15**, 511 (2003).
98. J. Zhong, W. Zhao, L. Lan, J. Wang, J. Chen, and N. Wang, *Journal of Alloys and Compounds*, **592**, 213 (2014).
99. M. Xie and T. Song, *ECS Journal of Solid State Science and Technology*, **2**, R29 (2013).
100. M. Y. Sharonov, A. B. Bykov, V. Petricevic, and R. R. Alfano, *Optics Communications*, **231**, 273 (2004).
101. S. M. Kaczmarek, W. Chen, and G. Boulon, *Crystal Research and Technology*, **41**, 41 (2006).
102. P. Dorenbos, *Journal of Luminescence*, **111**, 89 (2005).
103. N. V. Kuleshov, V. P. Mikhailov, V. G. Scherbitsky, B. I. Minkov, T. J. Glynn, and R. Sherlock, *Optical Materials*, **4**, 507 (1995).
104. C. P. Poole and D. S. MacIver, *The Journal of Chemical Physics*, **41**, 1500 (1964).
105. A. Ellison, J. O. V. Oubridge, and K. S. W. Sing, *Transactions of the Faraday Society*, **66**, 1004 (1970).
106. A. Sugimoto, Y. Nobe, and K. Yamagishi, *Journal of Crystal Growth*, **140**, 349 (1994).
107. D. Jia, X.-j. Wang, E. van der Kolk, and W. M. Yen, *Optics Communications*, **204**, 247 (2002).
108. D.-S. Xing, M.-L. Gong, X.-Q. Qiu, D.-J. Yang, and K.-W. Cheah, *Materials Letters*, **60**, 3217 (2006).
109. L. C. V. Rodrigues, R. Stefani, H. F. Brito, M. C. F. C. Felinto, J. Hls, M. Lastusaari, T. Laamanen, and M. Malkamki, *Journal of Solid State Chemistry*, **183**, 2365 (2010).
110. X. Y. Chen, Z. Li, S. P. Bao, and P. T. Ji, *Optical Materials*, **34**, 48 (2011).
111. R. J. Wiglusz and T. Grzyb, *Optical Materials*, **36**, 539 (2013).
112. V. Singh, R. P. S. Chakradhar, J. L. Rao, and J.-J. Zhu, *Materials Chemistry and Physics*, **111**, 143 (2008).
113. V. Singh, R. P. S. Chakradhar, J. L. Rao, and D.-K. Kim, *Journal of Luminescence*, **129**, 130 (2009).
114. P. Dorenbos, *Journal of Luminescence*, **136**, 122 (2013).
115. M. Kaneyoshi and E. Nakazawa, *Journal of The Electrochemical Society*, **152**, H80 (2005).
116. Y. Wu, G. Ren, D. Ding, S. Shang, D. Sun, G. Zhang, J. Wang, S. Pan, and F. Yang, *Journal of Luminescence*, **134**, 345 (2013).
117. X. Meng, S. Murai, K. Fujita, and K. Tanaka, *Journal of the Ceramic Society of Japan*, **116**, 1147 (2008).
118. L. I. Kazakova, G. M. Kuz'micheva, and E. M. Suchkova, *Inorganic Materials*, **39**, 959 (2003).
119. W. J. Schipper, J. J. Piet, H. J. De Jager, and G. Blasse, *Materials Research Bulletin*, **29**, 23 (1994).
120. Y. Hizhnyi, V. Chornii, S. Nedilko, M. Slobodyanik, I. Zatovsky, K. Terebilenko, and V. Boyko, *Radiation Measurements*, **56**, 397 (2013).
121. D. Van der Voort and G. Blasse, *Chemistry of Materials*, **3**, 1041 (1991).
122. H. E. Hoefdraad, F. M. A. Stegers, and G. Blasse, *Chemical Physics Letters*, **32**, 216 (1975).
123. Z.-J. Zhang, H.-H. Chen, X.-X. Yang, J.-T. Zhao, G.-B. Zhang, and C.-S. Shi, *Journal of Physics D: Applied Physics*, **41**, 105503 (2008).
124. Z.-J. Zhang, J.-L. Yuan, X.-J. Wang, D.-B. Xiong, H.-H. Chen, J.-T. Zhao, Y.-B. Fu, Z.-M. Qi, G.-B. Zhang, and C.-S. Shi, *Journal of Physics D: Applied Physics*, **40**, 1910 (2007).
125. M. Stiebler, C. Steudtner, and S. Kemmler-Sack, *Physica Status Solidi (a)*, **132**, 495 (1992).
126. G. Blasse and A. Bril, *Journal of Luminescence*, **3**, 109 (1970).
127. L. L. Noto, M. L. Chithambo, O. M. Ntwaeaborwa, and H. C. Swart, *Journal of Alloys and Compounds*, **589**, 88 (2014).
128. G. Blasse and A. Bril, *Journal of Solid State Chemistry*, **3**, 69 (1971).
129. L. H. Brixner and H.-y. Chen, *Journal of The Electrochemical Society*, **130**, 2435 (1983).
130. O. Voloshyna, S. V. Neicheva, N. G. Starzhinskiy, I. M. Zenya, S. S. Gridin, V. N. Baumer, and O. T. Sidletskiy, *Materials Science and Engineering: B*, **178**, 1491(2013).
131. X. Yin, Y. Wang, D. Wan, F. Huang, and J. Yao, *Optical Materials*, **34**, 1353 (2012).
132. P. Boutinaud, E. Cavalli, and M. Bettinelli, *Journal of Physics-Condensed Matter*, **19** (2007).
133. G. Martra, P. Vittone, S. Coluccia, F. Arena, and A. Parmaliana, *Il Nuovo Cimento D*, **19**, 1727 (1997).
134. C. C. Williams, J. G. Ekerdt, J. M. Jehng, F. D. Hardcastle, A. M. Turek, and I. E. Wachs, *The Journal of Physical Chemistry*, **95**, 8781(1991).
135. G. Blasse and A. Bril, *Journal of Inorganic and Nuclear Chemistry*, **29**, 2231 (1967).
136. Y. Wen, Y. Wang, F. Zhang, B. Liu, Z. Zhao, J. Zhang, and Z. Yang, *Journal of The Electrochemical Society*, **158**, J250 (2011).
137. C. C. Williams, J. G. Ekerdt, J. M. Jehng, F. D. Hardcastle, and I. E. Wachs, *The Journal of Physical Chemistry*, **95**, 8791(1991).
138. J.-j. Xie, Y. Shi, H. Yuan, H.-h. Cheng, W.-p. Wu, and J.-y. Liao, *physica status solidi (a)*, **206**, 121 (2009).
139. M. Mickens, Z. Assefa, and D. Kumar, *Journal of Sol-Gel Science and Technology*, **63**, 153 (2012).
140. T. Tian, Y. Kong, S. Liu, W. Li, L. Wu, S. Chen, and J. Xu, *Optics Letters*, **37**, 2679 (2012).
141. X. Cheng, X. Yu, B. Li, L. Yan, Z. Xing, and J. Li, *Materials Science and Engineering: B*, **178**, 425 (2013).
142. Z. Liu and Y. Chen, *Journal of Catalysis*, **177**, 314 (1998).
143. P. Dorenbos, *ECS Journal of Solid State Science and Technology*, **2**, R3001 (2013).
144. Z. Khan and M. Qureshi, *Catalysis Communications*, **28**, 82 (2012).
145. M. Winter, *The data were retrieved from the website webelements.com* (2014), URL http://www.webelements.com/.
146. B. Fricke, E. Johnson, and M. Rivera Glorivee, *Radiochimica Acta*, **62**, 17 (1993).
147. A. E. Kramida and J. Reader, *Atomic Data and Nuclear Data Tables*, **92**, 457 (2006).
148. E. G. Rogers and P. Dorenbos, *Journal of Luminescence*, **146**, 445 (2014).
149. E. G. Rogers and P. Dorenbos, *Journal of Luminescence*, , **155**, 135 (2014).
150. L. Pajasova, *Czechoslovak Journal of Physics B*, **19**, 1265 (1969).
151. A. Ohta, H. Nakagawa, H. Murakami, S. Higashi, and S. Miyazaki, *e-Journal of Surface Science and Nanotechnology*, **4**, 174 (2006).
152. M. Perego, G. Scarel, M. Fanciulli, I. L. Fedushkin, and A. A. Skatova, *Applied Physics Letters*, **90**, 162115(2007).
153. G. W. Gobeli and F. G. Allen, *Surface Science*, **2**, 402 (1964).
154. H. Friis, A. A. Finch, C. T. Williams, and J. M. Hanchar, *Physics and Chemistry of Minerals*, **37**, 333 (2010).
155. J. Robertson, *Journal of Non-Crystalline Solids*, **303**, 94 (2002).
156. A. V. Sidorenko, P. Dorenbos, A. J. J. Bos, C. W. E. van Eijk, and P. A. Rodnyi, *Journal of Physics: Condensed Matter*, **18**, 4503(2006).
157. Y. Wang, X. Guo, T. Endo, Y. Murakami, and M. Ushirozawa, *Journal of Solid State Chemistry*, **177**, 2242 (2004).
158. Y. Chen, B. Liu, C. Shi, M. Kirm, M. True, S. Vielhauer, and G. Zimmerer, *Journal of Physics: Condensed Matter*, **17**, 1217 (2005).
159. V. Y. Ivanov, V. A. Pustovarov, M. Kirm, E. S. Shlygin, and K. I. Shirinskii, *Physics of the Solid State*, **47**, 1492 (2005).
160. W. Drozdowski, A. J. Wojtowicz, D. Wisniewski, P. Szupryczynski, S. Janus, J.-L. Lefaucheur, and Z. Gou, *Journal of Alloys and Compounds*, **380**, 146 (2004).
161. J. Shmulovich, G. W. Berkstresser, C. D. Brandle, and A. Valentino, *Journal of The Electrochemical Society*, **135**, 3141 (1988).
162. D. Meiss, W. Wischert, and S. Kemmler-Sack, *physica status solidi (a)*, **133**, 575 (1992).
163. X. M. Han, J. Lin, J. Fu, R. B. Xing, M. Yu, Y. H. Zhou, and M. L. Pang, *Solid State Sciences*, **6**, 349 (2004).
164. Q. Lu and J. Li, *Optical Materials*, **33**, 381 (2011).
165. M. Yin, W. Zhang, L. Lou, S. Xia, and J. C. Krupa, *Physica B: Condensed Matter*, **254**, 141 (1998).
166. E. van der Kolk, P. Dorenbos, C. W. E. van Eijk, S. A. Basun, G. F. Imbusch, and W. M. Yen, *Physical Review B*, **71**, 165120 (2005).
167. D. Geng, G. Li, M. Shang, C. Peng, Y. Zhang, Z. Cheng, and J. Lin, *Dalton Transactions*, **41**, 3078 (2012).